Electronic materials

Check for updates

Three-dimensional AgNps@Mxene@PEDOT:PSS composite hybrid foam as a piezoresistive pressure sensor with ultra-broad working range

Ye Zhen[1], Vundrala Sumedha Reddy[1,*] (iD), Brindha Ramasubramanian[1], and
Seeram Ramakrishna[1]

[1] *Department of Mechanical Engineering, Centre for Nanotechnology and Sustainability, National University of Singapore, Singapore 119260, Singapore*

ABSTRACT

Piezoresistive pressure sensors are becoming increasingly popular for their applications in human motion detection, wearable electronics, health monitoring, and man–machine interfaces. Sensors with superior sensitivity and a broad range of sensing are desirable for practical implementation. To achieve those, a low-cost, scalable and simple fabrication technique of dip coating Ti_3C_2 (MXene), PEDOT:PSS, and AgNPs onto a melamine foam is proposed. The prepared sensor demonstrated sensitivity of 414.27 kPa^{-1} at (4.17–12.98 kPa), 182.52 kPa^{-1} at (12.98–94.55 kPa), 317.78 kPa^{-1} at (94.55 kPa–1.94 MPa), 164.32 kPa^{-1} at (> 1.94 MPa), extraordinaire detecting range 977.6 N and outstanding repeatability. The sensor was successfully applied for the real-time detection of heartbeat pulse, limb movement, human weight and powered an LED. Furthermore, an integrated circuit design with sensors had the ability to identify spatial pressure distribution and visualize it on a pressure map.

GRAPHICAL ABSTRACT
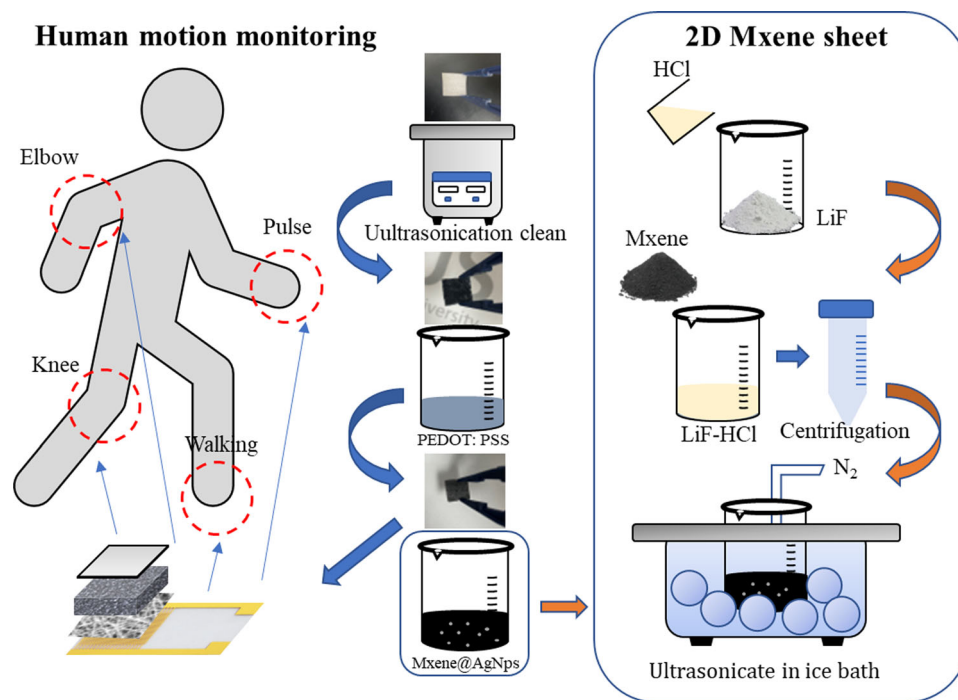
Introduction

For decades, people have been working on wearable technology. With the advancement of the electronic industry, wearable technology has reached its pinnacle [1]. Wearables combined with wireless and smartphone technologies can help in real-time monitoring of body movements, heartbeat, blood pressure, and other vital indications. Wearable technology is frequently used in health care due to these benefits. Wearable health devices help measure health indicators at home during early diagnosis, therapy, and post-treatment. It is easier to manage, minimizes the logistics of visiting the hospital, and saves time while being stress-less and hassle-free [2]. Sensors are essential in wearable technologies. These sensors, affixed to an individual's skin, detect and transmit impulses. Chemical and physical sensors are the most common types. Physical sensors offer information on bodily mobility, vibrations, pulses, etc. Chemical pressure utilizes the chemical reaction to affect the conductivity and further detect the pressure change [3]. Pressure sensors are typical physical wearable sensors with four distinct functioning mechanisms. Except these two types, bio-based pressure senor is another unique type pressure. Sensor is design based on bioreaction like immunoreaction[4–6], electrochemical reactions[7], chemical reaction[3]. The types of physical mechanisms involve piezoelectric [8], capacitive [9], triboelectric [10] and piezoresistive [11–14]. Among these, piezoresistive sensors have become increasingly popular due to their ease in the signal grouping, controllable sensing range, stability and applications in integrated devices, machine–human interface, healthcare monitoring etc. Piezoresistance came in 1856 (nineteenth century) when the change of resistance in copper and iron wires during elongation was discovered by William Thomson (Lord Kelvin) [15]. The piezoresistive effect was

introduced by Cookson in 1935, who defined it as the change in conductivity with stress [12].

Traditional piezoresistive sensors have been based on brittle sensing materials built on hard surfaces [13]. Following this, the properties of the next-generation piezoresistive sensors for wearable healthcare monitoring have been emphasized to have high flexibility, compressibility, stretchability, and bending capabilities, in addition to increased sensitivity. Sensitive sensing material selection and appropriate geometric electrodes should be used for a synergistic effect when designing such a piezoresistive sensor [14]. The basic principle behind the working of piezoresistive sensor mainly depends on the change in resistance of the material with varying external mechanical deformation. These sensors transform external force or pressure into current and resistance. [16]

Based on the material and device construction, a piezoresistive sensor can sense small vibrations in the human body, such as pulse, breath, and large stress or load. The flexible pressure sensor with high sensitivity, outstanding flexibility, and low cost can convert the external force information into electrical signals in real time [17, 18]. And it has potential to applied as electronic skin and healthcare detection systems for sensing biophysical signals such as pulse waves, respiration, and intraocular pressure [19]. Lot of soft material can play as the carrier of pressure sensor, such as polyurethane (TPU) substrate[19], poly (vinylidene fluoride) (PVDF)[20], cotton[6], polypyrrole (PPy) foam[18]. In this work, we choose commercial foam and used a low-cost and straightforward fabrication technique of dip coating for easily accessible foam.

Foam has a porous or fibrous structure with elasticity. It helps in obtaining high sensitivity to the wearable piezoresistive sensors. These criteria necessitate a series of fabrication processes, making large-scale production problematic. As a conventional material, foam can be found in our daily life, for example, as a foam washer, an acoustic absorber foam, a fireproof foam, a foam cushion etc. Due to the specific characteristics of the sponge, such as its energy absorption [21], elasticity [22], porosity [23], light-weightiness, low cost, and environmental friendliness, it acts as an ideal substrate for the wearable pressure sensor. By exploiting the porosity of the foam, piezoresistance can be induced by a series of steps involving carbonization [24], dipping-

coating [16, 25], followed by layer-by-layer assembly [26] of the sensor. These techniques facilitate compacting the foam while creating contact paths for current. Some recent research efforts are discussed to explore the current state-of-the-art. In 2018, Weijie et al.[24]. fabricated a carbonized (heat treatment to obtain carbon) foam at 800 °C in a nitrogen flow. It could detect slight pressure as low as 3 Pa. In addition to its 9 Pa detection limit, its endurance was remarkable, with 90% performance persisting after 11000 press-release cycles. Its performance can be linked to the carbon foam's flexible and soft character. Another easy procedure is dip-coating, which involves immersing the substrate in the material solution. Amit et al.[27]. demonstrated the working of reduced graphene oxide (rGO) based piezoresistive sensor. The sensor was fabricated by dipping polyurethane (PU) foams into rGO solution. Even after 5000 cycles of testing, there was almost no decrease in performance. It is profiting from 2-dimension (2D) material graphene, whose conductivity is better than 1-dimension (1D) material.

Moreover, 2D material can create a larger connect area facilitating the transfer of more electrons from one side to another. A different study involves free-standing graphene super light foam fabricated by Yarjan et al. [28]. Remarkably, a 30% compressive load on the foam increased its resistance to 120% of its initial value.

Mxene is a 2D material that has recently come to light. It was first reported by Naguib *et.al* in [29] Mxene can be produced by selectively etching MAX phase. MAX phase is the ternary carbides and nitrides with a $M_{n+1}AX_n$ formula. M is an early transition metal, A is an A-group (mostly groups 13 and 14) element, and X is C and/or N. In the present study, we are using Ti_3AlC_2 (MAX phase). The ultrathin Ti_3C_2 Mxene nanosheets are produced after acid etching process. The synthesis can be carried out by suspending a MAX phase in hydrofluoric acid (HF) [25, 30]. Due to the strong corrosivity of HF, Ghidiu et al. [31]. found an alternative synthesis technique which is easier and safe. The team immersed Ti_3AlC_2 in lithium fluoride (LiF) and concentrated aqueous hydrogen chloride (HCl) solution. 2D nanosheets were formed in ultrasonic treatment under protected gas flow. Mxene is a promising candidate for supercapacitor applications due to its excellent electrical conductivity and 2D structure [32], pressure sensor [33], battery electrode [34], electromagnetic

interference shielding [35], antibacterial activity [36], and in water and air purification [37]. Mxenes often have a negative charge due to the abundance of –OH, –O, and –F functional groups at their surface terminals [38]. Positively charged molecules are electrostatically adsorbed on the surface of Mxenes, providing the composite with improved sensing capabilities [39, 40].

In this work, we designed a robust piezoresistive melamine foam sensor. The foam was sequentially coated with PEDOT:PSS and Mxene. To further increase its conductivity, silver nanoparticles (Ag Nps) were mixed with Mxene solution. A simple dipping and coating approach was employed to prepare AgNps-Mxene@PEDOT:PSS sensor. It was possible to acquire a detection range that was greater than that of already accessible works [41, 42](from 0.417 to 817.8 N). This hybrid foam sensor can tolerate more than 90% deformation under a 977.6 N load, providing a stable response in a broad load range.

A comparison of various foam-based pressure sensor performances is listed in Table 1, showing the standing of our present work.
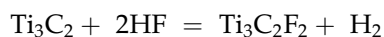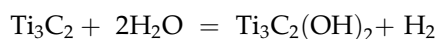
Experimental section

Materials

Commercially available Melamine sponge. Poly (3,4-ethylenedioxyiophene)-poly(styrenesulfonate) (PEDOT:PSS), Mxene (Ti_3AlC_2) power, Lithium fluoride (LiF) power, Sliver nanoparticle (AgNps) and Hydrochloric acid were purchased from Sigma-Aldrich (Singapore). The substrate used is commercially available melamine foam with 90% porosity. A simple dipping and coating method was used to fabricate Mxene@PEDOT:PSS@AgNps foam sensor. Step-wise fabrication of the composite foam has been discussed below.

Synthesis of 2D Mxene sheet

Mxenes are layered structures derived from MAX phase. Mxene sheets are synthesised by etching A-element atomic layers from the $M_{n+1}X_n$ adjacent layers from the MAX phase (i.e., Al layer in Ti_3AlC_2 is dissolved by acid). The etching process results in a terminated multi-layered Mxene powders with the 2D layers held together by hydrogen and van der Waals bonds [29, 47]. Layer "A" can be easily dissolved using hydrofluoric acid (HF)[29, 48, 49].

$$Ti_3AlC_2 + 3HF = AlF_3 + 3/2H_2 + Ti_3C_2$$

$$Ti_3C_2 + 2H_2O = Ti_3C_2(OH)_2 + H_2$$

$$Ti_3C_2 + 2HF = Ti_3C_2F_2 + H_2$$

Even in small quantities, HF remains dangerous. Considering the risk assessment and required safety procedures, severe corrosivity, we dissolved the A-layer using lithium fluoride-hydrochloric acid (LiF-HCl), instead of HF.

To obtain single- or few-layer Mxenes, sonication was performed and later replaced by intercalation of dimethyl sulfoxide (DMSO), which proved to be more efficient [50]. In this study, we solely synthesized multi-layered 2D Ti_3C_2X nanoflakes with intact structure for sensor application. To separate nanosheets, we used sonification procedure to increase the surface and contact area. To get a single layer nanosheet, it require more critical treatment. The beneficial impact of sonification has been discussed in subsequent section. Intensive processes are needed to produce a single-layer nanosheet.

Mxene nanosheets were fabricated by acid etching the Ti_3AlC_2 powder. Initially, 0.5 g Lithium Fluoride is added into 10 ml HCl (9 M) slowly and stirred for 10 min until LiF was completely dissolved. This step can produce LiF-HCl acid to react with Ti_3AlC_2 powder. In this solution, a total of 0.5 g Ti_3AlC_2 powder was added gradually in small amounts. This mixture was stirred continuously for 24 h at 40 °C on hot plate. Different HF acid concentration require different processing time for the complete reaction to happen. Mohamed Alhabeb et al. address this period under varied HF acid concentration. 5, 18, and 24 h for 30, 10, and 5 wt% HF, respectively. [47] The obtained solution was washed with deionized (DI) water and centrifuged at 4000 r/min for 10 min each time until the pH value was around 7 (the acceptable pH range is 5–7). After each centrifuge cycle, powder gets collected at the tube's bottom, drain the liquid. Then, add new DI water to the tube, until the PH level was maintained around 7. The Mxene powder settles at the bottom, and the top liquid was then drained off. Finally, to acquire a homogeneous Mxene aqueous dispersion, the resultant was placed into a three-necked, round-bottomed flask and ultrasonicated in an ice bath under protective nitrogen flow.

Table 1 Foam-based piezoresistive pressure sensors

Material	Fabrication method	Cycle of durability test	Detecting range	Sensitivity	Reference
Mxene@AgNps@PEDOT:PSS	Dip-coating	5000	4Kpa –8178Kpa (8.178 MPa)	414.27 kPa^{-1} at (4.17–12.98 kPa) 182.52 kPa^{-1} at (12.98–94.55 kPa) 317.78 kPa^{-1} at (94.55–1.94 MPa) 164.32 kPa^{-1} at (> 1.94 MPa)	Present work
Melamine foams	Carbonization at 800 degrees	11000	3 Pa–10 kPa	100.29 kPa^{-1}	[24]
Mxene	Dip-coating	10000	9 Pa–18.56 kPa	147 kPa^{-1} at (0–5.37 kPa) 442 kPa^{-1} at (5.37–18.56 kPa)	[16]
Chitosan@ Mxene	Dip-coating	5000	9pa–245.7 kPa	0.014 kPa^{-1} at (0–6.5 kPa) 0.015 kPa^{-1} at (6.5–85.1 kPa) 0.001 kPa^{-1} at (85.1–245.7 kPa)	[43]
Reduced graphene oxide (rGO)@ multiwalled carbon nanotubes (MWNTs)	Dip-coating	5000	2.22 − 16.4 kPa	0.022 kPa^{-1} at (0–2.7 kPa) 0.088 kPa^{-1} at (2.7–10.8 kPa) 0.034 kPa^{-1} at (10.8–48.8 kPa)	[27]
Polyurethane (TPU)@polydopamine (PDA)@MXene	combination of directional freezing and dip-coating method	5000	10 Pa–122.5 kPa	0.039 kPa^{-1} at (10–490 Pa) 0.0302 kPa^{-1} at (490 Pa–30 kPa) 0.0068 kPa^{-1} at (30–122.5 kPa)	[44]
Poly(3,4-ethylenedioxythiophene):poly-(styrenesulfonate) (PEDOT:PSS)	Dip-coating	1000	5.9–35 K pa	N.A	[42]
Silver nanowires (AgNWs)	Carbonization and Dipping-coating	1000	30–50 kPa	4.97 kPa^{-1}	[41]
Cellulose nanofiber @ carbon black (CNF@CB) conductive layer	Dip-coating	1000	Not mention-29Kpa	0.35 kPa^{-1} at (0–2.2 kPa) 0.082 kPa^{-1} at (2.2–7.9 kPa) 0.015 kPa^{-1} at (> 7.9 kPa)	[45]
Reduced graphene oxide (rGO)	Dip-coating	10 000 cycles, at 0–35 kPa	20 kPa–1.94 Mpa	0.0152 kPa^{-1}	[46]

Fabrication of AgNps-Mxene@PEDOT:PSS foam

Melamine was taken as a primary foam here with film (thickness is 2 mm) cut into 1 cm x 1 cm cube (size comparison with a 20 cents SGD coin (Fig. S1)). Firstly, the foam cube was washed with DI water. Secondly, it was dipped in the 95% ethyl alcohol and ultrasonicated for 20 min to get rid of unwanted foreign residue. Thirdly, rinsed and ultrasonicated while immersed in DI water for 20 min. Finally, the foam cube was dried in the oven at 60 °C for 4 h. The obtained clean foams were then dip-coated in 1.3wt% PEDOT:PSS solution. After the PEDOT:PSS coated foam was allowed to dry in the oven for 4 h, it was dipped in AgNps-Mxene solution. Forty milligram AgNps were added to 10 ml prepared Mxene nanosheet aqueous solution and stirred for 2 h to prepare AgNps-Mxene solution. PEDOT:PSS-coated foam was immersed into AgNps-Mxene solution and put in the vacuum oven at 30 °C for 24 h. Finally, it was then dried at 60 °C for 4 h to obtain the composite foam. The foam at different stages: plain, with PEDOT:PSS and AgNps-Mxene@PEDOT:PSS foam is shown from left to right in Fig S1.
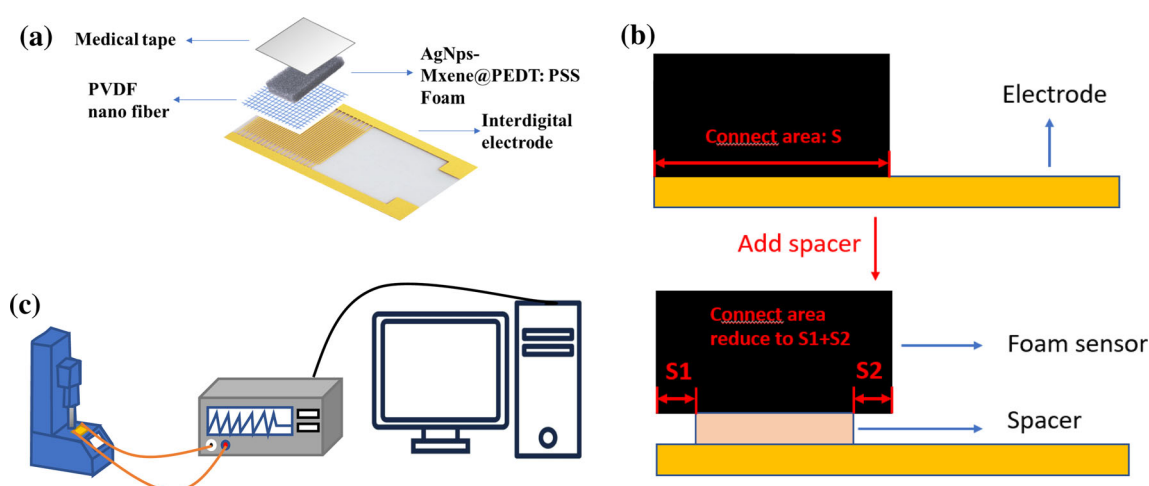
Assembly of AgNps-Mxene@PEDT:PSS foam pressure sensor

This foam sensor was assembled in a sandwich structure as shown in Fig. 1a. Bottom layer is an interdigital electrode, which was stacked with 0.5 cm*0.5 cm PVDF-HFP nanofiber spacer. Lastly,

AgNps-Mxene@PEDT:PSS foam was placed as the top layer. This sensor setup was sealed properly by biomedical transparent tape.

Nanofiber spacer

A pure PVDF-HFP nanofiber film fabricated by the electrospinning technique was utilized here. PVDF-HFP solution was prepared using the solvents acetone and N N-dimethylacetamide (DMAc) in the ratio of 1:1 with 16 wt% of PVDF-HFP pellets. The solution was vigorously stirred at room temperature for 48 h in order to obtain a homogeneous mixture. The solution was loaded into the syringe, and electrospinning was carried out while maintaining the parameters of 19 keV voltage, 200 rpm roller drum speed, collection width of 20 mm and a steady flow rate of 2 ml/hr. The spacer is a nonconductive layer which facilitates in separating of foam and electrode, drastically reducing the contact area Fig. 1b. The tensile test of PVDF-HFP nanofiber presented good elasticity and mechanical strength Fig S2.

We designed our experiments to discuss the effect of type and concentration of material. The layman's concept of piezoresistive sensors is that: in its usual form, the foam should be nonconducting, but when pressure is applied, it becomes conductive based on the additives and formation of conducting paths. PEDOT:PSS and Mxene are the essential materials in this case. Because of hydrophilicity and electrical conductivity, Mxene has a lower resistance at increasing concentrations. However, research has

Figure 1 **a** Schematic illustration of AgNps@Mxene@PEDT:PSS foam sensor assembly. **b** Work diagram of spacer. **c** The device testing set up.

shown that the performance of the sensor is restricted by Mxene concentration. The sensor's performance starts to decrease when the foam is highly concentrated by Mxene. This happens due to shorting with the interdigital electrode due to the complete conductivity of the foam. This limitation is addressed by the addition of a spacer layer.

We observed that Mxene powder is spilt from the foam structure during the pressure pressing procedure due to weak adherence of Mxene to the foam. As a result, the sensor became unstable and underperformed. In order to overcome his issue, we incorporated another conductive material PEDOT:PSS, which is in the liquid form that helps in adhering the particles. It can be easily absorbed and attaches tightly to the foam after drying. We added silver nanoparticles to increase the conductivity further as the insertion of a spacer eliminates the limitation of conductivity in sensor performance. Thus, the hybrid foam sensor was fabricated using step-by-step layer fabrication. In this study, we studied the effect of Mxene concentration while keeping the PEDOT:PSS concentration fixed. Three different concentrations of Mxene: 1 mg/ml, 2 mg/ml, 4 mg/ml were considered. The assembled device is shown in Fig. S3.

Result and discussion

Hybrid-coated foam

The conflict between high sensitivity and wide sensing range greatly limits the extensive application of flexible pressure sensors. To produce a sensor with both high sensitivity and wide range is still a challenging work. [51] In this work, we utilize the 2D-material Mxene to achieve a ultra-high sensitivity and detection range. The hybrid sensor is design based on a foam sensor. Commercial foam has a porous structure, which can be easily fabricated as a wearable sensor.

Sensitivity and detecting range are related to conductivity of our sensor. Figure 2c indicates the relationship between performance and conductivity (Mxene concentration). High conductivity further limits performance of sensor, as resistive response is necessary. Due to the limitation, we designed spacer layer. It can isolate foam and interdigital electrode to increase the detecting range (discussed in subsequent

section). We further introduce the silver nano particle (AgNps). As a conductive metal, silver can help to create conductive pathways, boost sensor sensitivity, and shorten response times simultaneously. It is commonly employed in sensors. *B.Cai et.al* achieved 4.97 kPa^{-1} sensitivity with a silver-coated carbonization foam. [41] Combination of Mxene and AgNps increase conductivity, but high concentration brings instability for sensor hence we controlled the composition. Both Mxene and AgNps are powder. The coated powder would disperse during compression or pressure application and the sensor's stability would be unable to achieve. In order to hold the components together, we introduced liquid phase, poly (3,4-ethylenedioxythiophene): poly (styrenesulfonic acid) (PEDOT:PSS), well-known as the most remarkable conducting polymer. Apart from coalition, the polymer also provides high transparency, tunable conductivity, excellent thermal stability and good film-forming properties. [52] As, after drying, the PEDOT:PSS thin film can attach on foam structure tightly. As a result of this combination, our hybrid foam sensor could present high sensitivity in ultra-high detecting range.

Pressure model and sensing properties of AgNps-Mxene@PEDT:PSS hybrid sensor

The piezoresistive properties are detected and tested by a group of the electrical signal test system and mechanical test setup present in Fig. 1c. The testing load range of the mechanical testing setup was 0.01–1000 N. The minimum detectable current of Keithley 2450 multi-source meter is 0.0001 nA. The sensitivity and performance of the fabricated sensor was calculated by using the equations below, and the respective abbreviations are given in Table 2.
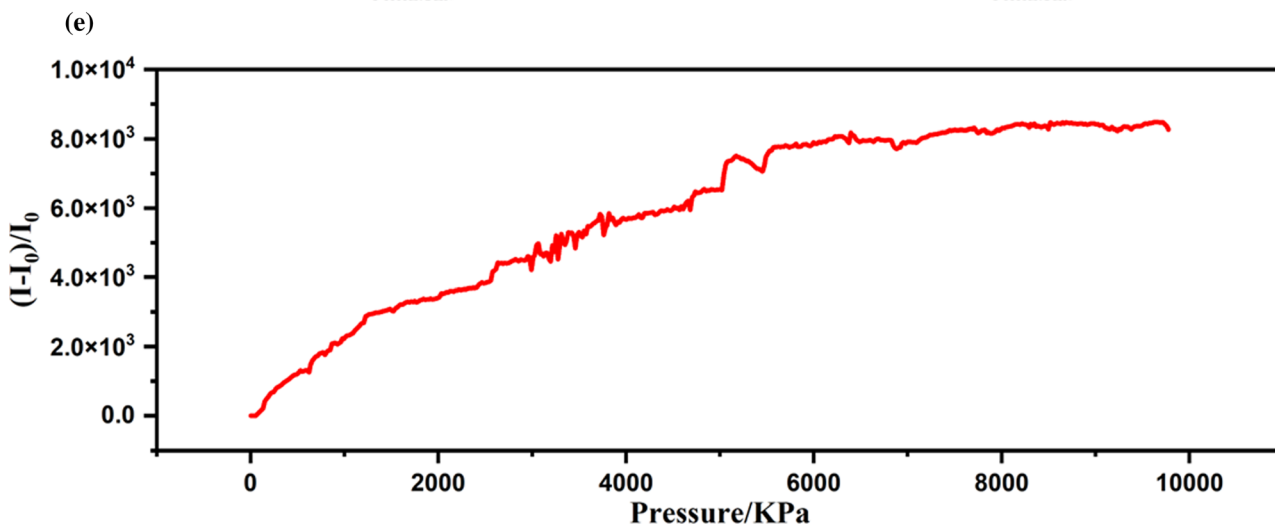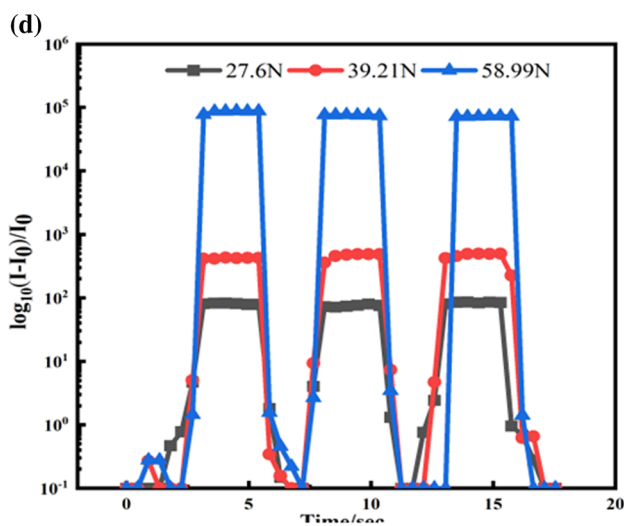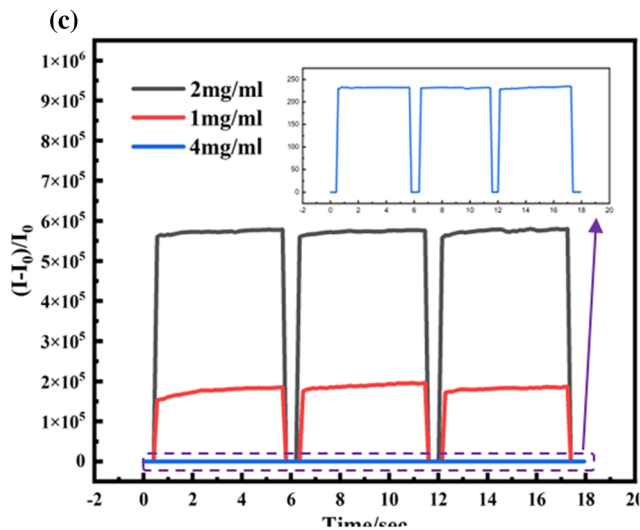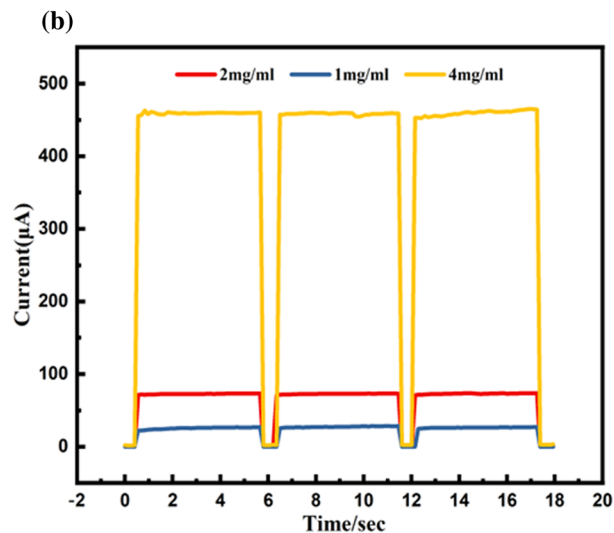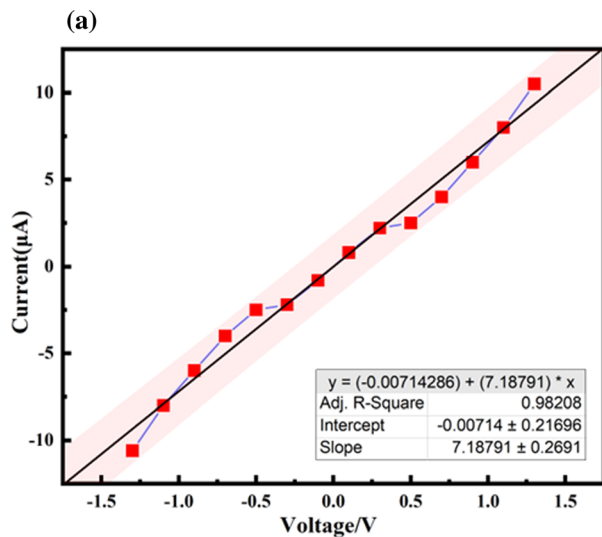
Performance

$$\text{Performance} = \frac{\Delta I}{I_0} \qquad (1)$$

$$\Delta I = I - I_0 \qquad (2)$$

Sensitivity

$$\text{Sensitivity} = \frac{\left(\frac{\Delta I}{I_0}\right)}{P} = \frac{\text{Performance}}{P} \qquad (3)$$

◀**Figure 2 a** I–V curve based on Mxene@PEDOT:PSS@AgNps sensor and its fitting curve. **b** Current present as y-axis for different concentration Mxene@PEDOT:PSS foam. **c** Performance present as y-axis for different concentration Mxene@PEDOT:PSS foam. **d** Different load pressure test, y-axis label is log10 due to high sensitivity. **e** Relationship between current and load. **f** Sensor response between 0 and 10 N **g**) Sensitivity of hybrid foam in different section **h**) Durability test, 5000 tests in total, only 1000 cycles are present here.

Table 2 Abbreviations of variables used in performance and sensitivity descriptions

Variable	Meaning
ΔI	Variable quantity of current
I	Testing current
I_0	Initial current
P	Pressure

Sensor assembly have already been mentioned before. Each sensor is appropriately sealed as an independent unit. Each unit was connected with an extending wire (connect by sliver paste) for testing (in order to keep a distance from the testing site to avoid any disturbance). The sensor unit is placed on the mechanical testing device holder. The electrode ends
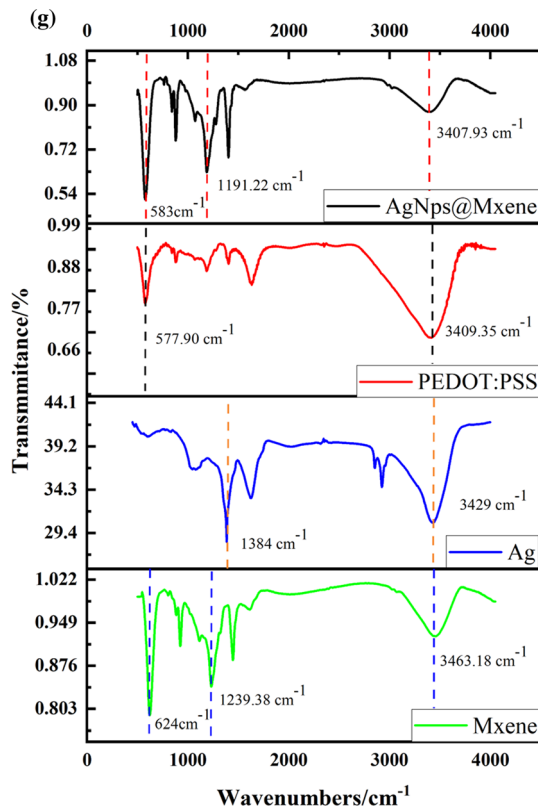

(f) **(g)** **(h)**
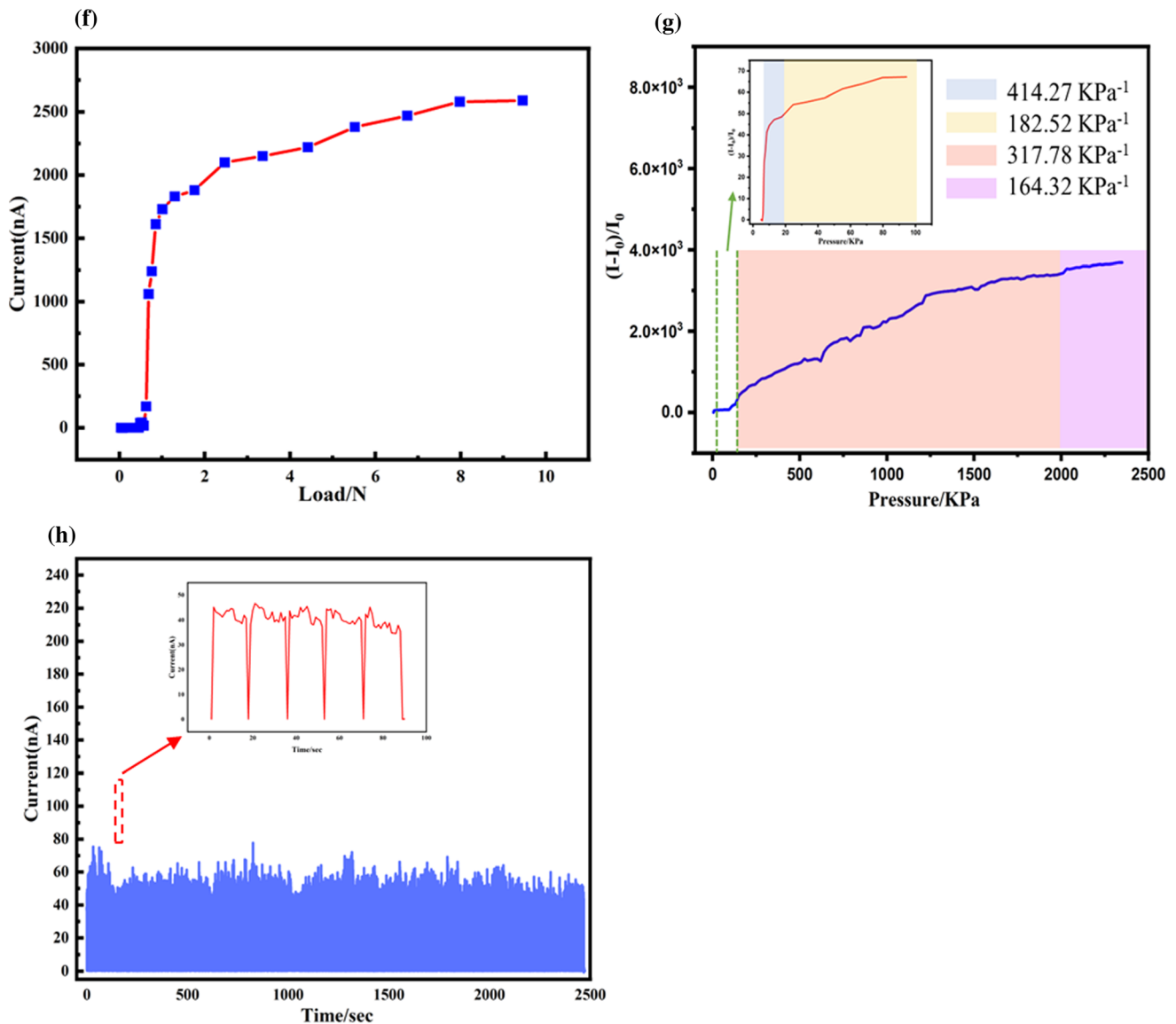
Figure 2 continued.

🌱 Springer
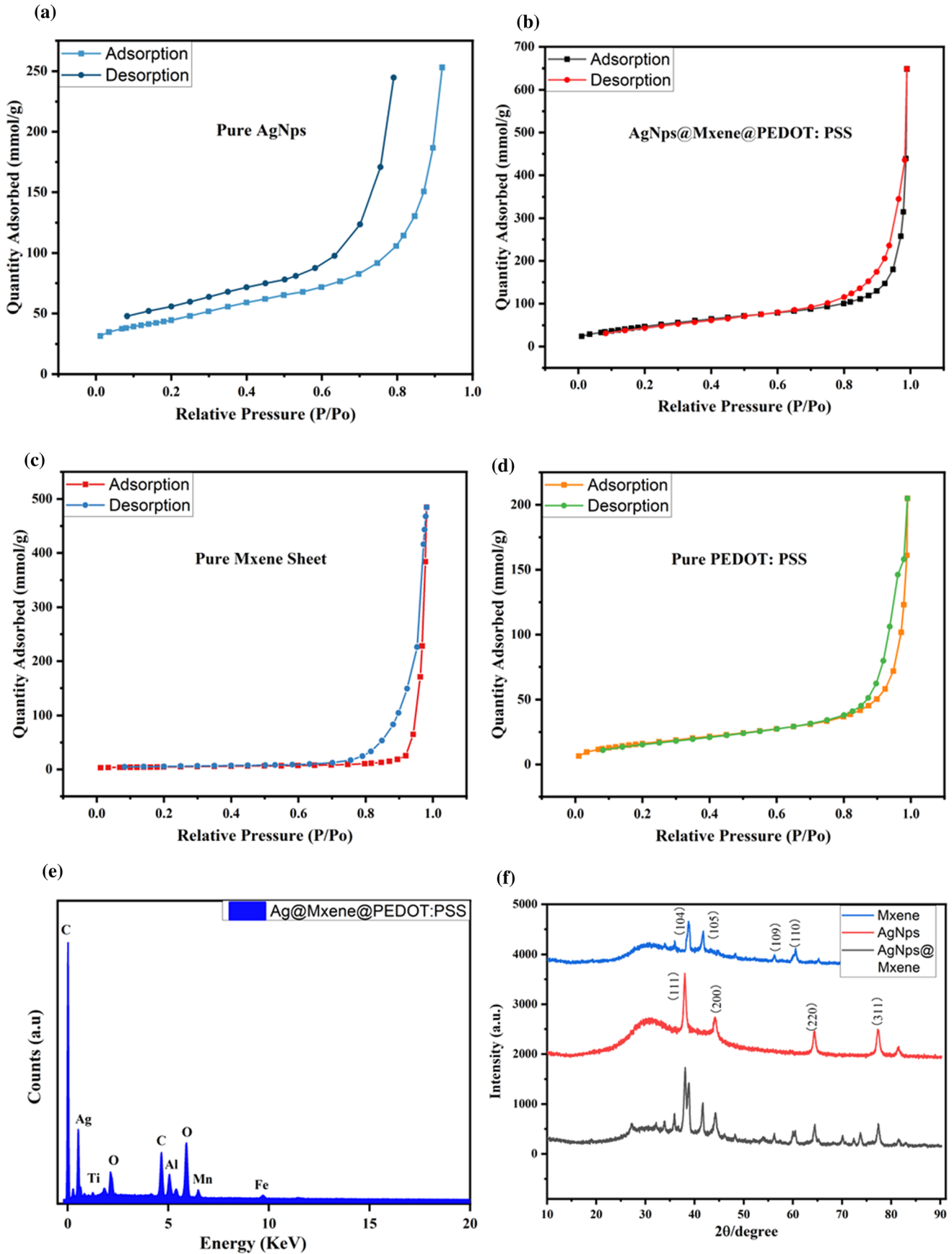
◀ **Figure 3 a** BET of pure AgNps. **b** Composite coating (AgNps@Mxene@PEDOT:PSS). **c** Pure Mxene sheet. **d** PEDOT:PSS . **e** EDX element analysis of hybrid foam sensor. **f** XRD analysis. **g** FTIR of coating material with various surface functionalization (scanned from 400 to 4500 cm^{-1}).


Figure 3 continued.

were connected to Keithley multi-source meter. All the current and other values are read by this measure meter. Both values on the source meter and mechanical testing setup are sent to the computer. All tests were conducted under external power (voltage). The standard testing voltage is 0.5 V, which is used as default in all the tests if not explicitly mentioned.

In Fig. 2a a linear relationship between voltage and current is observed after curve fitting, with voltage ranging from −1.5 to 1.5 V. Under the same load (28 N ± 3 N or pressure is 280 Kpa) and voltage (0.5 V), 4 mg/ml group showed the highest current value (up to 460 μA) as depicted in Fig. 2b. Concurrently, the current of 2 mg/ml group was 72 μA only, and there was a 435 μA gap between 4 and 1 mg/ml. The initial current of 4 mg/ml was higher than in other groups. The initial currents were $1.48*10^{-10}$,

$1.45*10^{-10}$, $1.97*10^{-06}$ nA for 1 mg/ml, 2 mg/ml, 4 mg/ml samples respectively. As displayed in Fig. 2c, 2mg/ml group showed the highest sensitivity ($\frac{\Delta I}{I_0}$) of $5.72043*10^5$, where the performance of 4 mg/ml sample only reached around 25. For each concentration, we prepared at least 4 samples. It was observed that, as concentration goes lower, the coating tends to be nonuniform. As a result, under the same concentration, different samples produced different performances. Hence due to inconsistency in the performance and sensitivity, they cannot be utilized as reliable sensors.

Here, the nanofiber spacer helps in increasing the detection range. The spacer can create a gap between the foam and the interdigital electrode. It can isolate them and reduce the connection points, which helps in further increasing the resistance of the whole unit. This phenomenon can be explained as follows. The resistance of the overall device may be categorized into two segments: (i) Contact resistance between MXene-sponge and electrode and (ii) MXene-sponge resistance. In a static state, adding the nanofiber enhances the interface contact resistance between the electrode and MXene-sponge, improving device functionality. The contact area between the MXene-sponge and the electrode is minimal without pressure, resulting in a comparatively low current. When an external force is exerted, the resistance of the MXene-sponge effectively reduces on one hand of the human. In contrast, on the other hand, the contact area between MXene-sponge and electrode expands significantly, lowering contact resistance and increasing the output current. The current change versus pressure curves may be separated into two linear regions: low-pressure and high-pressure regions [16]. Before we added the spacer, the initial current of 4 mg/ml sample was $1.97*10^{-06}$ nA. After introducing it, the current was reduced to $1.2*10^{-11}$ nA, increasing the detecting range immediately. The design of a spacer makes the high conductivity no longer a limitation to the sensor sensitivity. To further improve its sensitivity, we added silver nanoparticles to Mxene solution and fabricated the Mxene@PEDOT:PSS@AgNps sensor. Figure 2d presents the sensitivity of the hybrid foam under different loads. With introduction of the spacer and more conductive materials, the performance of hybrid foam is increasing dramatically (performance, $\frac{\Delta I}{I_0}$ is presented by log function). The sensitivity increased and the

Figure 4 **a** 3D structure of hybrid foam. **b** 2D Mxene sheet without ultrasonication. **c** Mxene sheets after ultrasonication. **d** Silver nanoparticles (AgNps). **e** AgNps and Mxene sheet attach on foam skeleton. **f** PVDF-HFP nanofiber network.
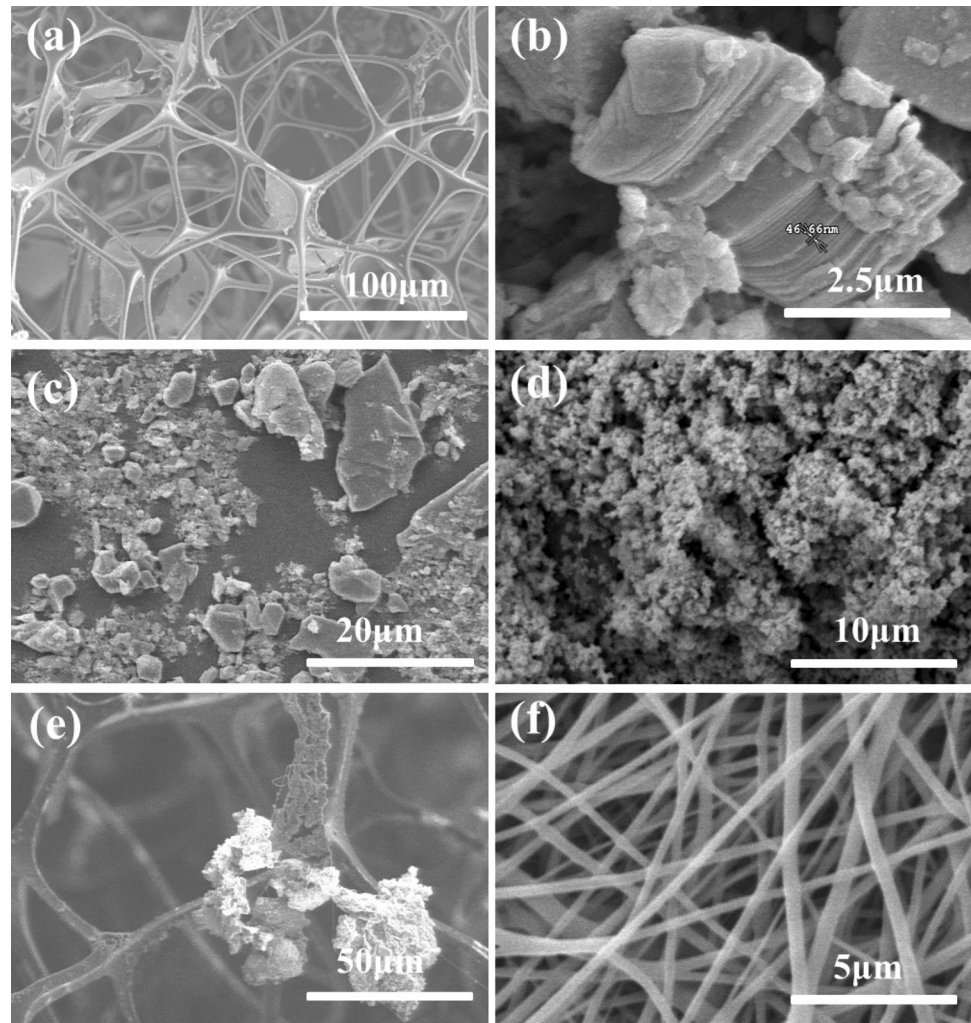

detection range drastically broadened when compared to other existing piezoresistive sensor. Load limit that the sample can bear reached 977.6 N (surface area of the sensor is 1 cm^2, equal to 9776 Kpa). This means that it can suffer an adult human weight easily. Figure 2e presents a curve between load and sensitivity. It was observed that when the load reached 700 N, the current increase rate was slower. When the load touched 817.8 N, the current almost hit the limit and stopped increasing.

Figure 2e also indicate that the increase of current almost follows a liner law. It can distinguish pressure levels clearly. In Fig. 2f it is represented that a minuscule load can also be detected by this sensor by using a more precise load meter of testing range between 0 and 10 N. The current was observed to go from 0.0558 to 0.37 nA and it kept increasing. The rapid increase of the current from 169 to 1060 nA in the beginning stops at 0.684 N. The current stabilizes and a steady increase when load

Figure 5 Hybrid foam sensor-based human body motion ▶ monitoring and heat map (**a**) finger press in different frequency (**b**) Front side elbow bending test (sensor is pasted on inner side of elbow). **c** Back side elbow bending test (sensor is pasted on outside of elbow). **d** Wrist band. **e** Finger banding angle detecting. **f** Real-time artificial pulse wave monitoring, plus here is 90 times per min. Hybrid foam sensor based human body motion monitoring and heat map. **g** Practical pressure map, start from circuit design to generate heat map.

surpass 0.684 N is observed. These results show high sensitivity in small load (0.417–0.684 N) and steady performance when applied a relatively higher load. To employ our sensor in different detecting ranges, we presented sensitivity ($\frac{(\Delta I/I_0)}{P}$) of sensor in each range Fig. 2g. It has been divided into four Sects. 414.27 K Pa^{-1} at (4.17–12.98 K Pa), 182.52 K Pa^{-1} at (12.98–94.55 K Pa), 317.78 K Pa^{-1} at (94.55 K Pa–1.94 M Pa), 164.32 K Pa^{-1}

(a)

(b)

(c)

(d)

(e)

(f)

(g)
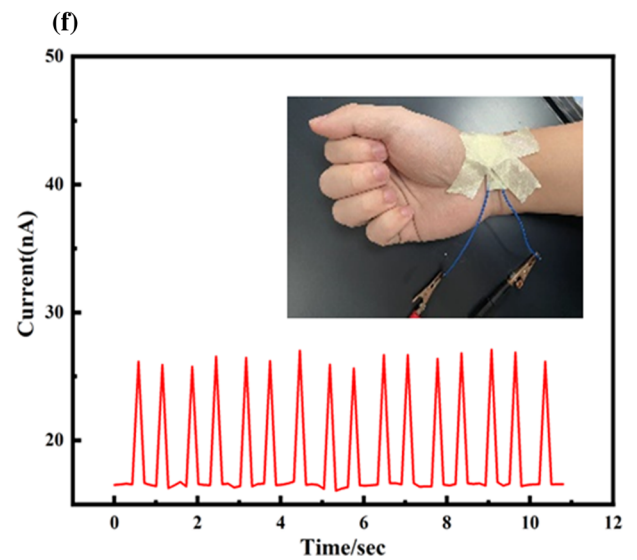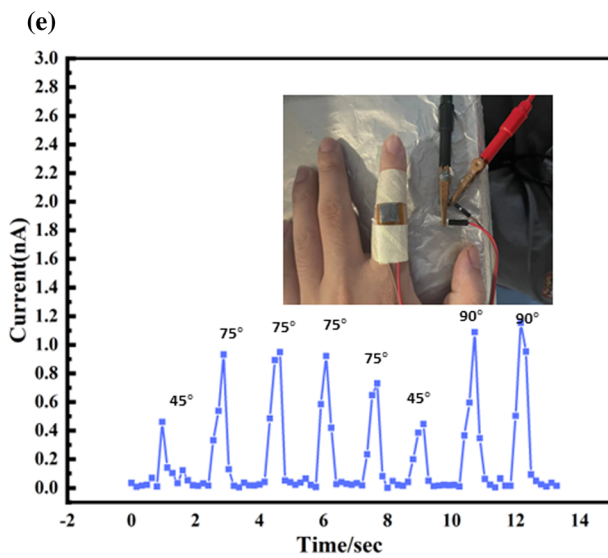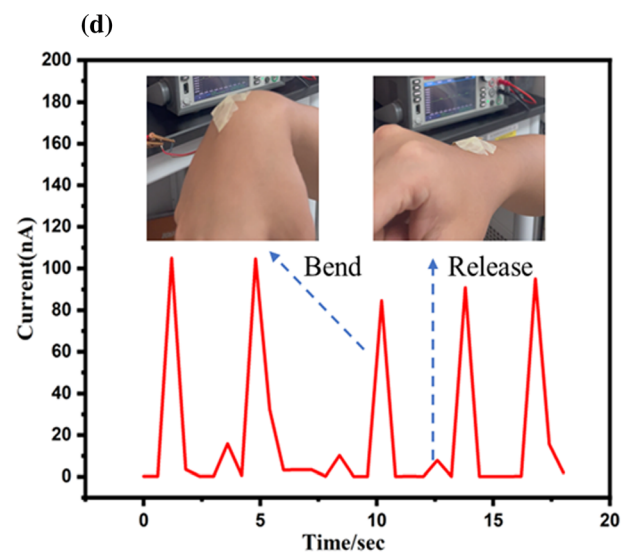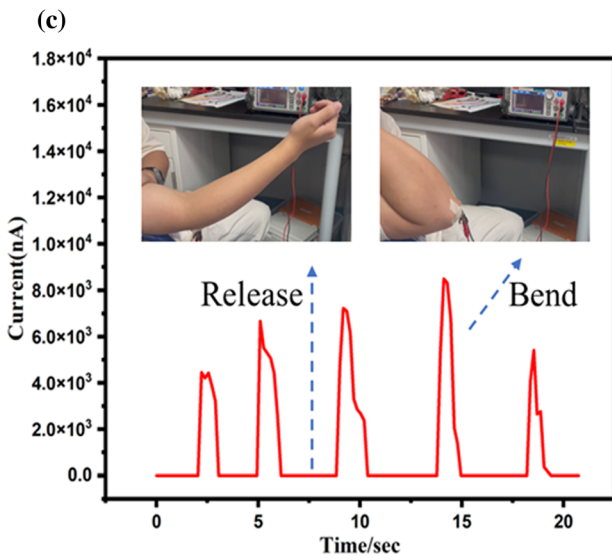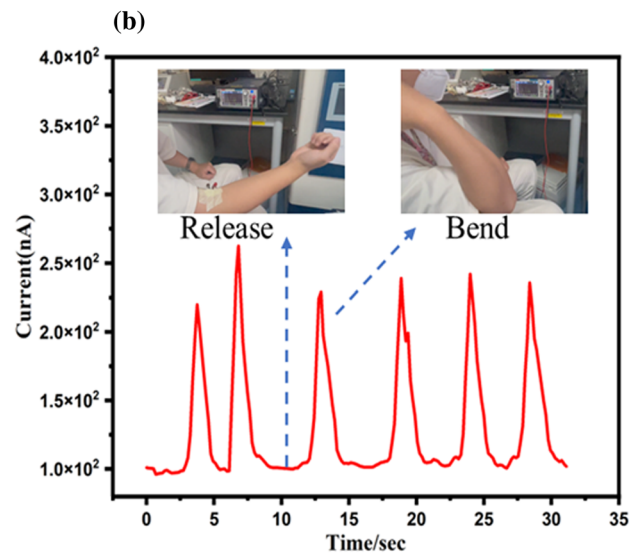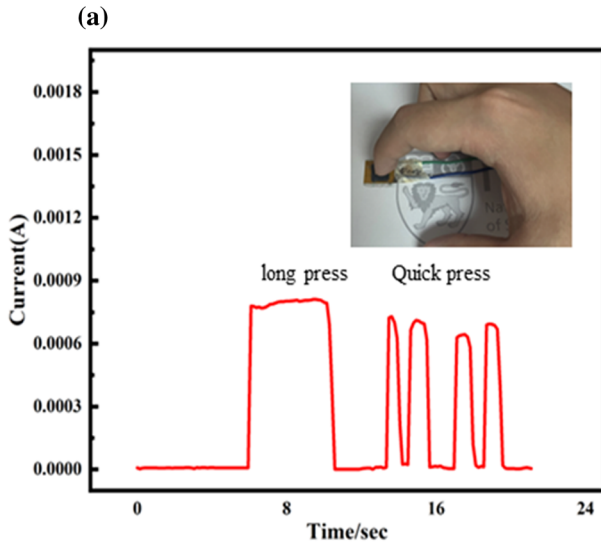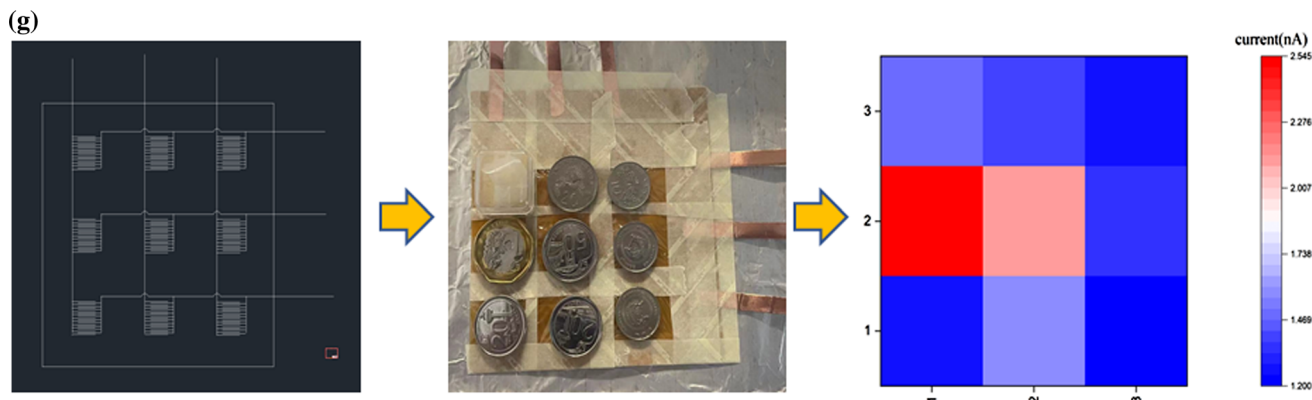
Figure 5 continued.

at (> 1.94 M Pa). In the most conventional range, 94.55 K Pa to 1.94 M Pa, our sample presented a relatively good sensitivity. The highest sensitivity was found in the lower pressure range (4.17–12.98 K Pa), which can facilitate accurate and clear detection of tiny press/motion. A durability test is essential to evaluate the sensor lifespan. The good elasticity of the foam allows it to withstand thousands of pressing-releasing cycles. Our present Mxene@PEDOT:PSS@AgNps sensor could endure more than 5000 cycles. We performed 5 rounds of durability tests with each round consisting of 1000 cycles. Figure 2h displays this durability test and proves that the sensitivity remains the same after 5000 cycles. The current signal exhibits little attenuation and approximately the same amount of current variation after each compressing–releasing cycle, indicating that the device is stable and has an extended operational life. Here the response time was also observed to be consistent over the whole load range.

Material characterization

BET surface area was calculated using the adsorption data in a relative pressure (P/P$_0$) range from 0.05 to 0.30. The total pore volume was assessed by converting the amount of nitrogen gas adsorbed at a relative pressure (P/P0) ≈ 0.99 to the volume of the liquid adsorbate. Pore size was calculated based on the adsorption isotherm by the Barret–Joyner–Halenda (BJH) model. The surface area was high for AgNps@Mxene@PEDOT:PSS ~ 1190.7 m^2/g as shown in Fig. 3a–d, with the pore size of 2.4 nm followed by 800.21 m^2/g for Mxene sheet, 253.2 m^2/g for Ag Nps [53, 54]. The impurity level was low in AgNps@Mxene@PEDOT:PSS, as shown in Fig. 3e,

Figure 6 **a** Grip test **b** Forward and backward motion monitoring ▶ (sensor is pasted on bottom of foot). **c** Human body weight detecting test. **d** Hybrid foam-based LED circuit (**e**–**f**) different pressure level applied on the foam sensor and its corresponding output.

with C, Ag, O and Ti corresponding to 64.81 wt%, 15.3 wt%, 8.4 wt%, 7.2 wt%. Traces of Mn, Fe and Al were also found [54].

To access the structure of the hybrid foam sensor with coating materials, powder XRD of Mxene, Ag nanoparticles and Mxene@AgNPs powder obtained from hybridization were performed. XRD patterns of ultrasonicated 2D nanosheets of Mxene had similar peaks to that of hybrid Mxene@AgNPs. The characteristic peaks of the MXene at (104), (105), and (110) are observed in Fig. 3f. [55]Ag NPs XRD pattern (Fig. 3f) confirmed the FCC structure is attributed to the (111), (200), (220), and (311) crystallographic planes of the face-centred cubic silver crystals showing peaks at 2θ of 38.18°, 44.25°, 64.72°, and 77.40°respectively [56]. As the coatings were to serve the purpose of distinct layers on the foam, there should not be any reaction among Mxene and Ag NPs. The lack of any other new peaks at AgNPs@Mxene confirmed the absence of chemical reaction and other impurities.

The functional groups of delaminated MXene, Ag NPs, PEDOT:PSS and AgNPs@Mxene were analyzed by FTIR in attenuated total reaction mode (Fig. 3g). Spectrum of MXene shows distinctive peaks at 624, 1239, and 3463 cm^{-1} corresponding to Ti–O, –COOH, and –OH groups. [55]. In Fig. 3g FTIR spectra of silver nanoparticles exhibited prominent peaks at 1384, and
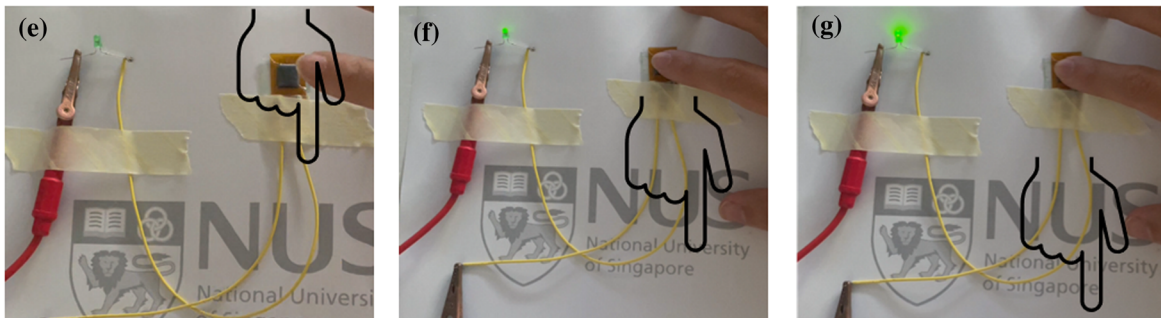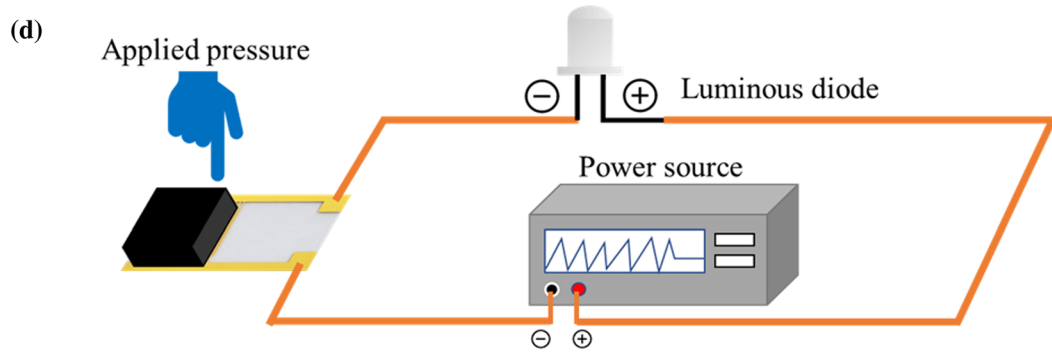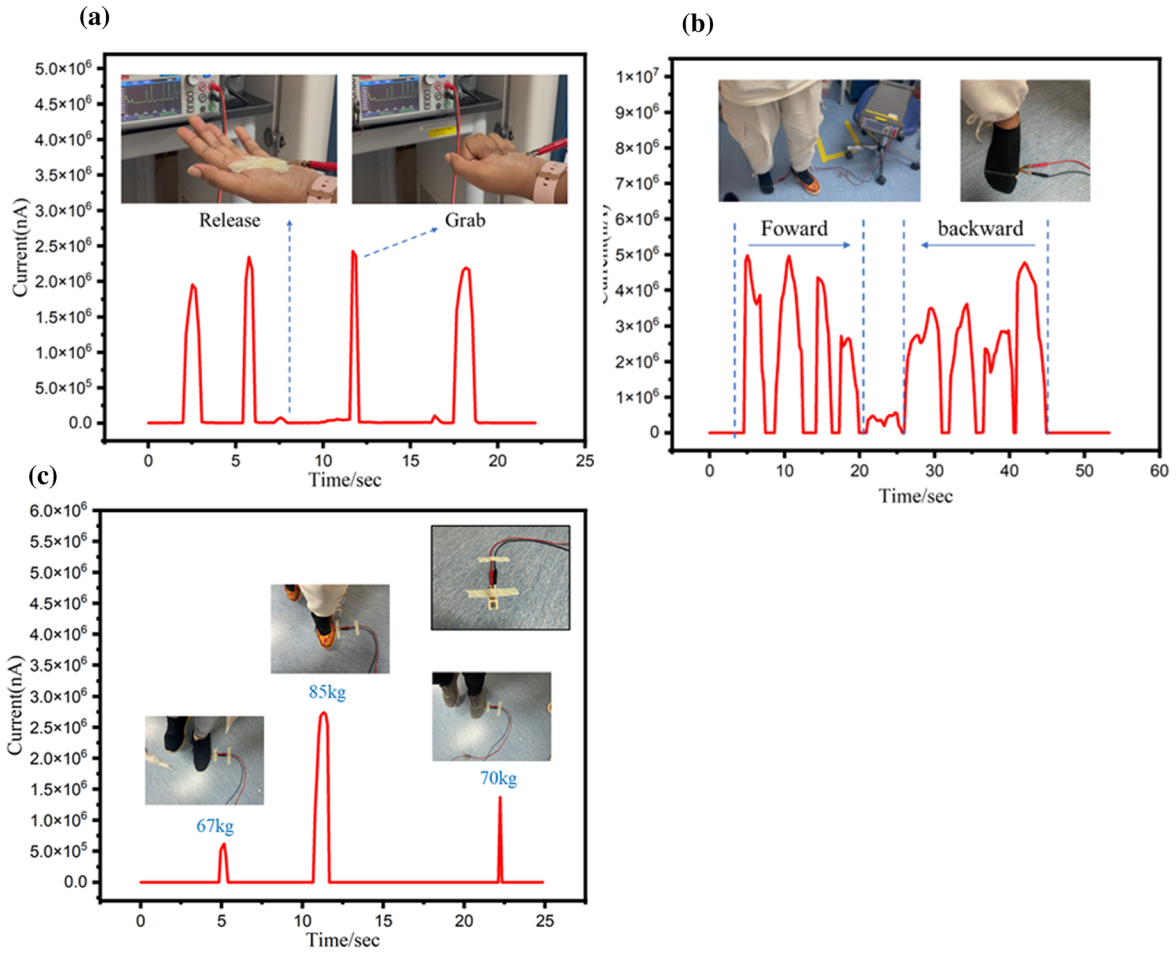
3429 cm^{-1}, corresponding to –H and C–C; C–N stretching [57]. PEDOT:PSS FTIR spectrum shows peaks at 578 and 3409 analogous to C–S and C = C stretching. The slight shift in the peak positions of AgNPs@Mxene attributes to the OH/H_2O adsorption.

The SEM image verifies the fiber network structure of the foam (Fig. 4a). Once the MAX phase is converted to Mxene, the Mxene sheets are stacked closely. This can be observed in Fig. 4b. They were then processed further to segregate the layers. Mxene 2D nanosheets that have been separated by ultrasonication have a larger surface area, as shown in Fig. 4c. Ag nanoparticles were evaluated to ensure equal distribution, lack of agglomeration, and moisture absorption (Fig. 4d). Figure 4e shows PEDOT:PSS, Mxene, and Ag nanoparticles coated and connected to a foam framework. Figure 4f shows the SEM image of a PVDF-HFP nanofiber spacer. The nanofiber's diameter was measured to be between 200 and 300 nm Fig S4.

AgNps@Mxene@PEDOT:PSS foam sensor for human motion monitoring and heat mapping

Benefitting from high sensitivity and detecting range, we employed the hybrid sensor for detecting human body motion ranging from tiny pressure of the pulse to as high as human weight. A random finger pressing test (pressing with different pressure, frequency and holding time) was carried out to verify the piezoresistive property of the foam (Fig. 5a). Sensor was placed at different joints of the human body; the location is placed inset to the readings. Relative to the bending and pressure suffered, varying current has been observed to be generated.

The type of force exerted by the human body is not singular but rather a complex mixture of pressure, strain, and torque, so we placed the sensor on the opposite side of the elbow as well as at the elbow along with the wrist and finger joints. The performance observed was an average peak of 2.2*10^2 nA (Fig. 5b), 7.0*10 nA (Fig. 5c) and 90 nA (Fig. 5d), respectively, for either side of the elbow and wrist joint. A clear depiction of varying output current with the difference in bending angle (45°, 75°, 90°) at the finger joint has been represented (Fig. 5e). For a 23-year-old male, a steady pulse was detected and noted to be 80 times/min approximately (Fig. 5f) which was within range of 70 to 90 times/min for a healthy human.

We have also designed a simple 3*3 matrix circuit with the interdigitated electrode to fabricate real-time 2D detection map, as shown in (Fig. 5g). We sealed 9 samples of Mxene@PEDOT:PSS@AgNps foam on this circuit to generate a pressure heat map. We put different coins and a tiny plastic container on top of each sample on the circuit. It was noticed that the current output was different when different loads were applied. The figure shows that pixelated sensor arrays are able to monitor the weight laid on the matrix. All the objects are taken from daily life, coins and plastic box possess different weights, and a corresponding heat map was generated. The coins chosen were from 10 cents to 1 Singapore dollar (SGD). One dollar coin is placed on the left side of the matrix, which is the heaviest. The height of each pi xel bar on a reconstructed map corresponding to the object distribution can be used to calibrate specific weight. This pressure sensor matrix might possibly be used in human–machine interactions, e.g., keyboards, especially super silent keyboards, since foam does not generate any noise.

We performed a series of pressure testing. The first one was the grip (squeeze) test presented in Fig. 6a. In the grip test by Mathiowetz V et al., they suggested that a healthy young woman aged between 20 and 24 could generate 70.4 pounds on average (equal to 313.28 N approximately) by grabbing, this was hundred times than finger joint bending. (in our testing, test by a young female student in this age range) [58]. A short and clean peak was observed in the test with a testing subject of a similar demographic Fig. 6a when we squeezed and released the hybrid foam sensor periodically. To further test the limit of our sensor, we performed walking tests and human body weight testing. As shown in Fig. 6b, the walking test was divided into two parts, forward and backward motion. The backward direction showed a broader peak because the hold time is usually higher (people are less skilled in walking backwards). Each step had a longer hold and the total walking period (numbers of steps are the same in both walking directions) was more as well. The detecting limit of our hybrid sensor is 977.6 N, which converts 97.76 kg. This detecting range is sufficient for human body weight detection. Three distinctive peaks in Fig. 6c correspond to different body weights 67 kg, 85 kg, 70 kg, respectively, of the subjects that took part in the experiment. One foot was lifted in the air, and we tried to apply whole body weight to the sensor.

Another test facilitating the piezoresistive property of the sensor is a continuously variable switch Fig. 6d. Sensor is the switch itself. The resistance of the sensor will change when the external force is applied. This property can control the current value in the circuit and further affect the brightness of the LED. Here, we designed a circuit to achieve this correlation of brightness and resistance. The change in brightness of the green LED diode with increasing pressure can be observed in Fig. 6e–g. Other colored LED diodes have also been tested, as shown in Fig. S5.

Conclusion

In summary, this hybrid sensor can be fabricated on a large scale with the facile dip-coating method, which is economical and quick. Due to the flexibility and elasticity of melamine foam, commercial melamine foam is used as the substrate to carry PEDOT:PSS@Mxene@AgNps mixture. Our sensor can be attached to human skin comfortably. And the unique structure with nanofiber spacer eliminates the limitation of conductivity, in turn providing a large detecting range for hybrid sensor (from 0.417 to 817.8 N). It was further verified by human body weight testing. At the same time, a low detection limit of 0.417 N allows the sensor to detect pulse steadily and easily. Based on these excellent characteristics of hybrid foam, we believe it can be utilized in the healthcare industry, such as human motion monitoring, weight measuring, and an electronic skin. Detailed fabrication process and working mechanism is provided in supplementary data.

Author contributions

YZ helped inconceptualization, methodology, writing original draft preparation. VSR contributed to writing writing-reviewing and editing, testing, investigation. BR performed resources, modifications. SR supervised the study.

Declarations

Conflict of interest There is no conflict of interests to disclose.

References

[1] Heikenfeld J, Jajack A, Rogers J, Gutruf P, Tian L, Pan T, Li R, Khine M, Kim J, Wang J, Kim J (2018) Wearable sensors: modalities, challenges, and prospects. Lab Chip 18:217–248. https://doi.org/10.1039/c7lc00914c

[2] Ghosh R, Pin KY, Reddy VS, Jayathilaka WADM, Ji D, Serrano-García W, Bhargava SK, Ramakrishna S, Chinnappan A (2020) Micro/nanofiber-based noninvasive devices for health monitoring diagnosis and rehabilitation. Appl Phys Rev 7:041309. https://doi.org/10.1063/5.0010766

[3] Zeng R, Wang W, Chen M, Wan Q, Wang C, Knopp D, Tang D (2021) CRISPR-Cas12a-driven MXene-PEDOT:PSS piezoresistive wireless biosensor. Nano Energy. https://doi.org/10.1016/j.nanoen.2020.105711

[4] Yu Z, Tang Y, Cai G, Ren R, Tang D (2019) Paper electrode-based flexible pressure sensor for point-of-care immunoassay with digital multimeter. Anal Chem 91:1222–1226. https://doi.org/10.1021/acs.analchem.8b04635

[5] Yu Z, Cai G, Tong P, Tang D (2019) Saw-toothed microstructure-based flexible pressure sensor as the signal readout for point-of-care immunoassay. ACS Sens 4:2272–2276. https://doi.org/10.1021/acssensors.9b01168

[6] Huang L, Zeng Y, Liu X, Tang D (2021) Pressure-based immunoassays with versatile electronic sensors for carcinoembryonic antigen detection. ACS Appl Mater Interfaces 13:46440–46450. https://doi.org/10.1021/acsami.1c16514

[7] Cho H, Lee H, Lee S, Kim S (2021) Reduced graphene oxide-based wearable and bio-electrolyte triggered pressure sensor with tunable sensitivity. Ceram Int 47:17702–17710. https://doi.org/10.1016/j.ceramint.2021.03.090

[8] McGinn CK, Kam KA, Laurila M-M, Montero KL, Mäntysalo M, Lupo D, Kymissis I (2020) Formulation, printing, and poling method for piezoelectric films based on PVDF–TrFE. J Appl Phys 128:225304. https://doi.org/10.1063/5.0027855

[9] Tan Z, Shalmany SH, Meijer GCM, Pertijs MAP (2012) An energy-efficient 15-bit capacitive-sensor interface based on

period modulation. IEEE J Solid-State Circuits 47:1703–1711. https://doi.org/10.1109/JSSC.2012.2191212

[10] Wang X, Zhang H, Dong L, Han X, Du W, Zhai J, Pan C, Wang ZL (2016) Self-powered high-resolution and pressure-sensitive triboelectric sensor matrix for real-time tactile mapping. Adv Mater 28:2896–2903. https://doi.org/10.1002/ADMA.201503407

[11] Traite M, Welkowitz W, Downs R (1960) Intracardiac catheter tip piezoresistive pressure gauge. Rev Sci Instrum 31:987–991. https://doi.org/10.1063/1.1717125

[12] Cookson JW (1935) Theory of the piezo-resistive effect. Phys Rev 47:194. https://doi.org/10.1103/PhysRev.47.194.2

[13] Suhling JC, Jaeger RC (2001) silicon piezoresistive stress sensors and their application in electronic packaging. IEEE Sens J 1:14

[14] Ma Y, Liu N, Li L, Hu X, Zou Z, Wang J, Luo S, Gao Y (2017) A highly flexible and sensitive piezoresistive sensor based on MXene with greatly changed interlayer distances. Nature Commun. https://doi.org/10.1038/s41467-017-01136-9

[15] Thomson W (1857) XIX. On the electro-dynamic qualities of metals:—effects of magnetization on the electric conductivity of nickel and of iron. Proc R Soc Lond 8:546–550. https://doi.org/10.1098/RSPL.1856.0144

[16] Yue Y, Liu N, Liu W, Li M, Ma Y, Luo C, Wang S, Rao J, Hu X, Su J, Zhang Z, Huang Q, Gao Y (2018) 3D hybrid porous Mxene-sponge network and its application in piezoresistive sensor. Nano Energy 50:79–87. https://doi.org/10.1016/j.nanoen.2018.05.020

[17] Zang Y, Zhang F, Di CA, Zhu D (2015) Advances of flexible pressure sensors toward artificial intelligence and health care applications. Mater Horiz 2:140–156. https://doi.org/10.1039/c4mh00147h

[18] Yu Z, Cai G, Liu X, Tang D (2020) Platinum nanozyme-triggered pressure-based immunoassay using a three-dimensional polypyrrole foam-based flexible pressure sensor. ACS Appl Mater Interfaces 12:40133–40140. https://doi.org/10.1021/acsami.0c12074

[19] Huang L, Zeng R, Tang D, Cao X (2022) Bioinspired and multiscale hierarchical design of a pressure sensor with high sensitivity and wide linearity range for high-throughput biodetection. Nano Energy. https://doi.org/10.1016/j.nanoen.2022.107376

[20] Zhu L, Lv Z, Yin Z, Li M, Tang D (2021) Digital multimeter-based point-of-care immunoassay of prostate- specific antigen coupling with a flexible photosensitive pressure sensor. Sens Actuators B Chem. https://doi.org/10.1016/j.snb.2021.130121

[21] Han F, Seiffert G, Zhao Y, Gibbs B (2003) Acoustic absorption behaviour of an open-celled aluminium foam. J Phys D Appl Phys 36:294. https://doi.org/10.1088/0022-3727/36/3/312

[22] Warren WE, Kraynik AM (1997) Linear elastic behavior of a low-density kelvin foam with open cells. J Appl Mech 64:787–794. https://doi.org/10.1115/1.2788983

[23] Sang G, Zhu Y, Yang G, Zhang H (2015) Preparation and characterization of high porosity cement-based foam material. Constr Build Mater 91:133–137. https://doi.org/10.1016/J.CONBUILDMAT.2015.05.032

[24] Liu W, Liu N, Yue Y, Rao J, Luo C, Zhang H, Yang C, Su J, Liu Z, Gao Y (2018) A flexible and highly sensitive pressure sensor based on elastic carbon foam. J Mater Chem C Mater 6:1451–1458. https://doi.org/10.1039/c7tc05228f

[25] Lin B, Yuen ACY, Li A, Zhang Y, Chen TBY, Yu B, Lee EWM, Peng S, Yang W, Lu HD, Chan QN, Yeoh GH, Wang CH (2020) MXene/chitosan nanocoating for flexible polyurethane foam towards remarkable fire hazards reductions. J Hazard Mater. https://doi.org/10.1016/j.jhazmat.2019.120952

[26] Liu Q, Gao S, Zhao Y, Tao W, Yu X, Zhi M (2021) Review of layer-by-layer self-assembly technology for fire protection of flexible polyurethane foam. J Mater Sci 56(16):9605–9643. https://doi.org/10.1007/S10853-021-05904-3

[27] Tewari A, Gandla S, Bohm S, McNeill CR, Gupta D (2018) Highly exfoliated mwnt-rgo ink-wrapped polyurethane foam for piezoresistive pressure sensor applications. ACS Appl Mater Interfaces 10:5185–5195. https://doi.org/10.1021/ACSAMI.7B15252/SUPPL_FILE/AM7B15252_SI_002.AVI

[28] Novel Graphene Foam Composite with Adjustable Sensitivity, (n.d.).

[29] Naguib M, Kurtoglu M, Presser V, Lu J, Niu J, Heon M, Hultman L, Gogotsi Y, Barsoum MW (2011) Two-dimensional nanocrystals produced by exfoliation of Ti 3AlC 2. Adv Mater 23:4248–4253. https://doi.org/10.1002/adma.201102306

[30] Naguib M, Kurtoglu M, Presser V, Lu J, Niu J, Heon M, Hultman L, Gogotsi Y, Barsoum MW (2011) Two-Dimensional nanocrystals produced by exfoliation of Ti3AlC2. Adv Mater 23:4248–4253. https://doi.org/10.1002/ADMA.201102306

[31] Conductive two-dimensional titanium carbide 'clay,' (n.d.).

[32] Hu M, Li Z, Li G, Hu T, Zhang C, Wang X (2017) All-solid-state flexible fiber-based MXene supercapacitors. Adv Mater Technol 2:1700143. https://doi.org/10.1002/ADMT.201700143

[33] Guo Y, Zhong M, Fang Z, Wan P, Yu G (2019) A wearable transient pressure sensor made with MXene nanosheets for sensitive broad-range human-machine interfacing. Nano Lett

19:1143–1150. https://doi.org/10.1021/ACS.NANOLETT.8B04514/SUPPL_FILE/NL8B04514_SI_001.PDF

[34] Shao H, Xu K, Wu YC, Iadecola A, Liu L, Ma H, Qu L, Raymundo-Piñero E, Zhu J, Lin Z, Taberna PL, Simon P (2020) Unraveling the charge storage mechanism of Ti3C2T xmxene electrode in acidic electrolyte. ACS Energy Lett 5:2873–2880. https://doi.org/10.1021/ACSENERGYLETT.0C01290/SUPPL_FILE/NZ0C01290_SI_006.AVI

[35] Sun R, Binzhang H, Liu J, Xie X, Yang R, Li Y, Hong S, Yu ZZ (2017) Highly conductive transition metal carbide/carbonitride(MXene)@polystyrene nanocomposites fabricated by electrostatic assembly for highly efficient electromagnetic interference shielding. Adv Funct Mater. https://doi.org/10.1002/adfm.201702807

[36] Rasool K, Mahmoud KA, Johnson DJ, Helal M, Berdiyorov GR, Gogotsi Y (2017) Efficient antibacterial membrane based on two-dimensional Ti3C2Tx (MXene) nanosheets. Sci Rep. https://doi.org/10.1038/s41598-017-01714-3

[37] Xie X, Chen C, Zhang N, Tang ZR, Jiang J, Xu YJ (2019) Microstructure and surface control of MXene films for water purification. Nature Sustain 2(9):856–862. https://doi.org/10.1038/s41893-019-0373-4

[38] Khazaei M, Arai M, Sasaki T, Chung CY, Venkataramanan NS, Estili M, Sakka Y, Kawazoe Y (2013) Novel electronic and magnetic properties of two-dimensional transition metal carbides and nitrides. Adv Funct Mater 23:2185–2192. https://doi.org/10.1002/ADFM.201202502

[39] Ma Z, Li S, Wang H, Cheng W, Li Y, Pan L, Shi Y (2019) Advanced electronic skin devices for healthcare applications. J Mater Chem B 7:173–197. https://doi.org/10.1039/C8TB02862A

[40] Xin M, Li J, Ma Z, Pan L, Shi Y (2020) MXenes and their applications in wearable sensors. Front Chem. https://doi.org/10.3389/fchem.2020.00297

[41] Cai B, Wang L, Yu F, Jia J, Li J, Li X, Yang X, Jiang Y, Lu W (2021) Compressible piezoresistive pressure sensor based on Ag nanowires wrapped conductive carbonized melamine foam. Appl Phys A 128(1):1–8. https://doi.org/10.1007/S00339-021-05143-Y

[42] Ding Y, Yang J, Tolle CR, Zhu Z (2018) Flexible and compressible PEDOT:PSS@Melamine conductive sponge prepared via one-step dip coating as piezoresistive pressure sensor for human motion detection. ACS Appl Mater Interfaces 10:16077–16086. https://doi.org/10.1021/ACSAMI.8B00457/SUPPL_FILE/AM8B00457_SI_006.AVI

[43] Li XP, Li Y, Li X, Song D, Min P, Hu C, bin Zhang H, Koratkar N, Yu ZZ (2019) Highly sensitive, reliable and flexible piezoresistive pressure sensors featuring polyurethane sponge coated with MXene sheets. J Colloid Interface Sci 542:54–62. https://doi.org/10.1016/j.jcis.2019.01.123

[44] Chen Q, Gao Q, Wang X, Schubert DW, Liu X (2022) Flexible, conductive, and anisotropic thermoplastic polyurethane/polydopamine /MXene foam for piezoresistive sensors and motion monitoring. Compos Part A Appl Sci Manuf 155:106838. https://doi.org/10.1016/J.COMPOSITESA.2022.106838

[45] Xu S, Li X, Sui G, Du R, Zhang Q, Fu Q (2020) Plasma modification of PU foam for piezoresistive sensor with high sensitivity, mechanical properties and long-term stability. Chem Eng J 381:122666. https://doi.org/10.1016/J.CEJ.2019.122666

[46] Lü X, Yu T, Meng F, Bao W (2021) Wide-range and high-stability flexible conductive graphene/thermoplastic polyurethane foam for piezoresistive sensor applications. Adv Mater Technol 6:2100248. https://doi.org/10.1002/ADMT.202100248

[47] Alhabeb M, Maleski K, Anasori B, Lelyukh P, Clark L, Sin S, Gogotsi Y (2017) Guidelines for synthesis and processing of two-dimensional titanium carbide (Ti3C2Tx MXene). Chem Mater 29:7633–7644. https://doi.org/10.1021/acs.chemmater.7b02847

[48] Cai G, Yu Z, Tong P, Tang D (2019) Ti3C2 MXene quantum dot-encapsulated liposomes for photothermal immunoassays using a portable near-infrared imaging camera on a smartphone. Nanoscale 11:15659–15667. https://doi.org/10.1039/c9nr05797h

[49] Chen J, Tong P, Huang L, Yu Z, Tang D (2019) Ti3C2 MXene nanosheet-based capacitance immunoassay with tyramine-enzyme repeats to detect prostate-specific antigen on interdigitated micro-comb electrode. Electrochim Acta 319:375–381. https://doi.org/10.1016/j.electacta.2019.07.010

[50] Mashtalir O, Naguib M, Mochalin VN, Dall'Agnese Y, Heon M, Barsoum MW, Gogotsi Y (2013) Intercalation and delamination of layered carbides and carbonitrides. Nat Commun. https://doi.org/10.1038/ncomms2664

[51] Xiang Y, Fang L, Wu F, Zhang S, Ruan H, Luo H, Zhang H, Li W, Long X, Hu B, Zhou M (2021) 3D Crinkled Alk-Ti3C2 MXene based flexible piezoresistive sensors with ultra-high sensitivity and ultra-wide pressure range. Adv Mater Technol. https://doi.org/10.1002/admt.202001157

[52] Shi H, Liu C, Jiang Q, Xu J (2015) Effective approaches to improve the electrical conductivity of PEDOT:PSS: a review. Adv Electron Mater. https://doi.org/10.1002/aelm.201500017

[53] Le TA, Tran NQ, Hong Y, Kim M, Lee H (2020) Porosity-engineering of mxene as a support material for a highly efficient electrocatalyst toward overall water splitting.

Chemsuschem 13:945–955. https://doi.org/10.1002/CSSC.201903222

[54] Subbaiyan R, Ganesan A, Ramasubramanian B (2022) Self-potent anti-microbial and anti-fouling action of silver nanoparticles derived from lichen-associated bacteria. Appl Nanosci 2022:1–12. https://doi.org/10.1007/S13204-022-02501-X

[55] Karthikeyan P, Elanchezhiyan SS, Preethi J, Talukdar K, Meenakshi S, Park CM (2021) Two-dimensional (2D) Ti3C2Tx MXene nanosheets with superior adsorption behavior for phosphate and nitrate ions from the aqueous environment. Ceram Int 47:732–739. https://doi.org/10.1016/J.CERAMINT.2020.08.183

[56] Shameli K, Bin Ahmad M, Zamanian A, Sangpour P, Shabanzadeh P, Abdollahi Y, Zargar M (2012) Green biosynthesis of silver nanoparticles using curcuma longa tuber powder. Int J Nanomed 7:5603–5610. https://doi.org/10.2147/IJN.S36786

[57] Devaraj P, Kumari P, Aarti C, Renganathan A (2013) Synthesis and characterization of silver nanoparticles using cannonball leaves and their cytotoxic activity against MCF-7 cell line. J Nanotechnol. https://doi.org/10.1155/2013/598328

[58] Mathiowetz V, Kashman N, Volland G, Weber K, Dowe M,.Rogers S Grip and pinch strength: normative data for adults, (n.d.).